metals

MDPI

Review

A Short Review on Welding and Joining of High Entropy Alloys

João G. Lopes and João Pedro Oliveira *

UNIDEMI, Department of Mechanical and Industrial Engineering, NOVA School of Science and Technology, Universidade NOVA de Lisboa, 2829-516 Caparica, Portugal; jcg.lopes@campus.fct.unl.pt

* Correspondence: jp.oliveira@fct.unl.pt; Tel.: +351-21-294-96-18

Received: 27 December 2019; Accepted: 31 January 2020; Published: 2 February 2020

Abstract: High entropy alloys are one of the most exciting developments conceived in the materials science field in the last years. These novel advanced engineering alloys exhibit a unique set of properties, which include, among others, good mechanical performance under severe conditions in a wide temperature range and high microstructural stability over long time periods. Owing to the remarkable properties of these alloys, they can become expedite solutions for multiple structural and functional applications. Nevertheless, like any other key engineering alloy, their capacity to be welded, and thus become a permanent feature of a component or structure, is a fundamental issue that needs to be addressed to further expand these alloys' potential applications. In fact, welding of high entropy alloys has attracted some interest recently. Therefore, it is important to compile the available knowledge on the current state of the art on this topic in order to establish a starting point for the further development of these alloys. In this article, an effort is made to acquire a comprehensive knowledge on the overall progress on welding of different high entropy alloy systems through a systematic review of both fusion-based and solid-state welding techniques. From the current literature review, it can be perceived that welding of high entropy alloys is currently gaining more interest. Several high entropy alloy systems have already been successfully welded. However, most research works focus on the well-known CoCrFeMnNi. For this specific system, both fusion and solid-state welding have been used, with no significant degradation of the joints' mechanical properties. Among the different welding techniques already employed, laser welding is predominant, potentially due to the small size of its heat source. Overall, welding of high entropy alloys is still in its infancy, though good perspectives are foreseen for the use of welded joints based on these materials in structural applications.

Keywords: welding; high entropy alloys; laser welding; friction stir welding; microstructure; review

1. Introduction

Throughout recent years, high entropy alloys (HEAs) have arisen as a new reality in the advanced materials domain. The motivation behind this innovative class of engineering materials was based on the purpose of broadening the boundaries of knowledge in what concerns alloys with more than one main constituent. This concept can be traced back to 2004, when the first papers concerning this subject were published [1,2], whereas, at the present time, several other works [3–12] have also been presented to extend the available information regarding HEAs.

Currently, a common definition for these alloys was introduced by one of the precursor works, where high entropy alloys are described as metallic compounds with at least five principal elements, with the percentage of each component varying between 5 and 35 at.% [2]. However, other definitions include a wider range of materials, with different component amounts, which can also be considered

high entropy alloys [3]. Several review papers address and discuss the different nomenclatures regarding high entropy alloys [3,13–17], and as such, we refrain from addressing this topic in this paper.

As established by Yeh [18], these innovative multi-element compositions confer to these materials four distinct core effects:

The "high entropy effect", associated to the high configurational entropy that stabilizes the formation of simple solid-state phases such as body-centered-cubic (BCC) or face-centered-cubic (FCC), while inhibiting the development of brittle intermetallic compounds. However, it must be noted that high entropy alloys can still exhibit brittle-like behavior, as evidenced for the AlCoCrCuFeNi system [19].

The "lattice distortion effect", that occurs due to the lack of a dominant element in the composition of the alloy, resulting in different atoms of different sizes occupying the lattice positions of the crystal structure, promoting its distortion and affecting the physical and mechanical properties of the alloy. Depending on the selected atomic elements and their concentration, distinct phases, with potentially different mechanical properties can form as evidenced in the work of Wu et al. [20]. As such, the lattice distortion effect can be used to promote a phase over the other for specific alloy systems. Recent work by He et al. [21] has shown that not only the atomic ratio of the element that compose the high entropy alloy affect the lattice distortion, but the alloy Poisson ration must also be considered.

The "sluggish diffusion effect", that constrains the atomic diffusion of the elements and inhibits the phase transformations that require such phenomenon to occur. As a result, higher recrystallization temperatures can be achieved, and formation of nano-precipitates and amorphous structures are susceptible to occur, as such, second-phase precipitation only occurs after extremely long periods [22]. Bhattacharjee et al. [23] showed that heat treatments with the duration of 1 h at or below 800 °C in severely deformed CoCrFeNiMn high entropy alloys would not result in any significant grain growth. However, when the temperature was of 900 or 1000 °C, massive grain growth was observed. Regarding the extremely long times and temperatures required for second-phase precipitation, Pickering et al. [22] showed that annealing at 700 °C for times above 500 h would lead to the formation of $M_{23}C_6$ and σ phase.

The "cocktail effect", which refers to the enhancement of the established properties of the alloy, which cannot be attributed independently to any of the elements that compose the material [24].

Considering the above-mentioned features and the prospect of customizing the composition of high entropy alloys, a new path for a wide range of applications can be expected. As such, owing to these properties, the outstanding performance of HEAs to operate under extreme conditions is subjected to intensive research. Depending on the composition of the alloy, the corrosion resistance [25–28], the ability to sustain high cyclical loading [29,30], wear resistance [31–33], and the good performance at both high [34,35] and cryogenic temperatures [36–38] are some of the key features that these alloys exhibit towards being novel solutions for structural and functional applications [39]. Miracle et al. [40] suggest that high entropy alloys can be used as structural materials in transportation and energy sectors. The same author [41] proposes that some high entropy alloys can be used in functional applications that require resistance to radiation damage or when in need of diffusion barriers, as in the microelectronics sector. Replacement of conventional materials by entropy alloys is suggested to occur in the future, and materials to be replaced include stainless steels, Al-, Ti-, and Ni-based alloys. This is related to the fact that high entropy alloys can be fine-tuned to simultaneously present, if desired, low density and high mechanical strength or other combination of properties. These properties will be dictated by the elements that compose the high entropy alloy system. Table 1 summarizes the mechanical properties (yield stress, ultimate tensile stress, and elongation) for multiple high entropy alloy systems at different temperatures.

Table 1. Mechanical properties of various high entropy alloys (HEAs) under different temperatures.

Alloy System	Mechanical Properties	Temperature (K)									Refs.
		77	296	673	873	1073	1273	1473	1673	1873	
CoCrFeNiMn	σ_{ys} (MPa)	759	410	-	-	-	-	-	-	-	[42]
	σ_{uts} (MPa)	763	1280	-	-	-	-	-	-	-	
	Elongation (%)	71	57	-	-	-	-	-	-	-	
CoCrFeMn	σ_{ys} (MPa)	481	272	-	-	-	-	-	-	-	[38]
	σ_{uts} (MPa)	1003	567	-	-	-	-	-	-	-	
	Elongation (%)	65	47	-	-	-	-	-	-	-	
CoCrFeNiAl	σ_{ys} (MPa)	-	250	155	150	-	-	-	-	-	[43]
	σ_{uts} (MPa)	-	-	-	-	-	-	-	-	-	
	Elongation (%)	-	>50	>50	>50	-	-	-	-	-	
CrFeNiMnAl	σ_{ys} (MPa)	-	910	755	325	-	-	-	-	-	[43]
	σ_{uts} (MPa)	-				-	-	-	-	-	
	Elongation (%)	-	>50	>50	>50	-	-	-	-	-	
CoCrFeNiAlTi	σ_{ys} (MPa)	-	1420	1285	795	285	-	-	-	-	[43]
	σ_{uts} (MPa)	-	-	-	-	-	-	-	-	-	
	Elongation (%)	-	18	24	>50	>50	-	-	-	-	
CrFeNiMnAlTi	σ_{ys} (MPa)	-	1280	1100	355	-	-	-	-	-	[43]
	σ_{uts} (MPa)	-				-	-	-	-	-	
	Elongation (%)	-	31	>50	>50	-	-	-	-	-	
CoCrFeNiV	σ_{ys} (MPa)	477	470	-	-	-	-	-	-	-	[37]
	σ_{uts} (MPa)	1000	626	-	-	-	-	-	-	-	
	Elongation (%)	62	36	-	-	-	-	-	-	-	
HfNbTaTiZrW	σ_{ys} (MPa)	-	1550	-	-	577	409	345	-	-	[44]
	σ_{uts} (MPa)	-		-	-				-	-	
	Elongation (%)	-	26.3	-	-	>35	>35	>35	-	-	
HfNbTaTiZrMoW	σ_{ys} (MPa)	-	1637	-	-	1065	736	703	-	-	[44]
	σ_{uts} (MPa)	-		-	-				-	-	
	Elongation (%)	-	15.5	-	-	>35	>35	>35	-	-	
HfNbTaTiZr	σ_{ys} (MPa)	-	929	790	675	535	295	92	-	-	[45]
	σ_{uts} (MPa)	-	-	-	-	-	-	-	-	-	
	Elongation (%)	-	-	-	-	-	-	-	-	-	
VNbMoTaW	σ_{ys} (MPa)	-	1246	-	862	846	842	735	656	477	[46]
	σ_{uts} (MPa)	-	1270	-	1597	1536	1454	943	707	479	
	Elongation (%)	-	1.7	-	13	17	19	7.5			
NbMoTaW	σ_{ys} (MPa)	-	1058	-	561	552	548	506	421	405	[46]
	σ_{uts} (MPa)	-	1211	-	-	-	1008	803	467	600	
	Elongation (%)	-	-	-	-	-	-	-	-	-	

To ensure the viability of these alloys to be used in complex shaped structures, their weldability is an important issue that needs to be addressed. Any advanced engineering alloy will require welding to either obtain complex shape structures or to couple its properties to those from another material. As such, evaluating the weldability of novel alloys is fundamental to further expand its potential applications. Additionally, because these alloys are now being more studied, it is possible to adjust their chemistry or microstructure to avoid weldability issues, such as liquation cracking. The sooner these potential issues are found, the easier and more cost-effective it is to find a solution.

This paper analyses the overall progress achieved using well-known welding techniques and weldability studies on HEAs. First, focus is given to fusion-based techniques, in a second instance, a review of solid-state ones is provided.

2. Current Progress on Welding HEAs

Among several methods for joining materials, welding comprises a broad range of techniques, and it is an expedite and often a reliable way to produce permanent and continuous joints. When proper design specifications and process optimization are used, welding technologies become unquestionably competitive for several industrial sectors, such as infrastructure construction and transportation. This category of processes is known to be capable of achieving particularly strong and resistant bonds when exposed to static and dynamic forms of loading [47,48]. As such, welding technologies can be divided according to the diverse mechanisms and processes required to achieve such joints.

Fusion-based welding processes are based on melting and solidification of metal and are currently the most established in industry. The resultant joints are typically characterized by exhibiting three distinct regions. The fusion zone (FZ), which is the region that undergoes melting and subsequent solidification; the heat affected zone (HAZ), that is characterized by experiencing temperatures that can promote solid-state transformation and never changes its state (i.e., the material never becomes fully liquid during the process); and, lastly, the base material (BM), which is the region that remains unchanged throughout the process.

Often, fusion-based welding methods are known to impair the mechanical properties of the joints due to metallurgical incompatibility between the materials to be joined, development of high residual stresses, mismatch of thermomechanical properties of the BMs, or due to the sensitivity of the material to the weld thermal cycle. In those cases, solid-state techniques are a viable option capable of solving some of the above-mentioned problems. One well-known example is dissimilar welding of aluminium to steels [49]: While fusion welding can be used to join this dissimilar combination, the resulting mechanical properties are often poor due to the formation of brittle intermetallic compounds upon mixing of the liquid phases of the two BMs. However, solid-state methods can effectively join these materials allowing their use in structural applications.

Solid-state welding is based on intense friction, plastic deformation, and diffusion mechanisms that aid in the formation of a joint between the BMs [50]. The versatility of such approach is proven by the ability to connect materials that are difficult or impossible to join through fusion-based processes, avoiding the development of undesired phases, distortions, and high residual stresses that may occur during the liquid-solid state interchange. These processes where plastic deformation occurs, exhibit a thermomechanically affected zone (TMAZ), as well as an HAZ. The microstructural evolution of the joints will depend on the material susceptibility to the combined effect of temperature and deformation in the TMAZ, and of temperature in the HAZ.

Another possibility for materials joining is through brazing and soldering. These are mainly characterized by the introduction of a filler metal into the joint region. In such processes, the metallic filler has a melting point lower than that of the materials that are to be welded, and the welds are established by diffusion between the filler and BMs [47].

Regarding the overall developments of welding of HEAs, a survey on the contemporary literature shows that an effort is being made towards the understanding of the microstructural evolution and optimization of these joining processes [51]. Until now, the number of publications regarding welding of HEAs is increasing throughout the years, as the developments on these alloys become more evident, as it can be observed in Figure 1.

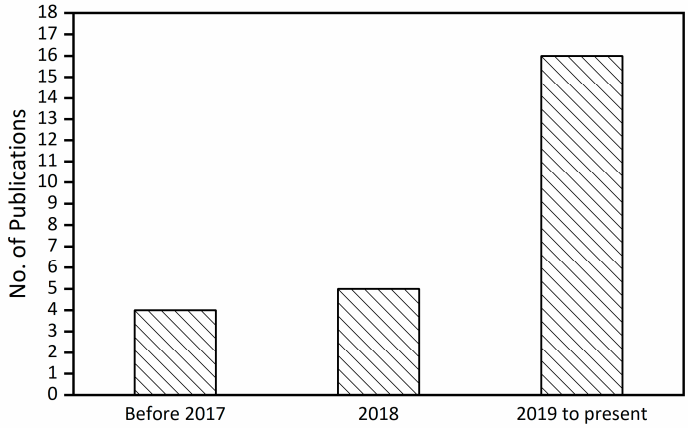

Figure 1. Number of publications on welding of high entropy alloys over time.

However, to the best of the authors' knowledge, most studies are focused on fusion-based welding processes. Still, it is also possible to perceive that some efforts are also being dedicated to the study

of other welding techniques on HEAs, especially in what concerns solid-state welding processes. Considering this, the next topics that are presented in this paper mainly concern the overall progress on fusion-based and solid-state welding processes on HEAs. Nevertheless, information about welding HEAs through brazing is also available, as presented by Lin et al. [52], where dissimilar joints between CoCrFeMnNi/CoCrFeNi alloy and CoCrFeMnNi/316 stainless steel were investigated.

2.1. Fusion-based Welding of HEAs

Several studies [53–69] have already been reported on fusion-based welding of HEAs. To date, these works focus mainly on laser-based techniques, although some information is also available on Electron Beam and Gas Tungsten Arc Welding (GTAW) techniques.

In terms of the materials, the most used HEA is the CoCrFeNiMn one. This is probably related to the fact that this alloy system is the most studied within the field of HEAs [22,25,34,70–72]. For this reason, in this section of the paper (2.1.1), we first address the current status on fusion-welding of the CoCrFeNiMn HEA system, and the following one (2.1.2) focuses on the remaining materials that were already welded.

2.1.1. CoCrFeNiMn HEA System

Concerning the investigation of the welded joints behavior on HEAs obtained through laser-based techniques, Kashaev et al. [53] reported a study on the CoCrFeNiMn system, where the base material was fabricated via self-propagating high temperature synthesis, a process where reagents are ignited and then, due to an exothermic reaction, a given product is formed [73]. The as-produced HEA exhibited columnar FCC grains with MnS precipitates and Cr-rich carbides on its microstructure, and, as a consequence of the BM manufacturing method, its matrix composition revealed a reduced content of Mn and the existence of several impurities. These impurities did not lead to any strengthening effect, most likely due to their large grain size and low volume fraction. After welding, using a laser power of 2 kW and a welding speed of 5 m/min, several changes in texture and microstructure of the FCC matrix occurred. The precipitation of nanoscale intermetallic B2 phase compounds in the welded region promoted an increase of the microhardness in the fusion zone, as evidenced in Figure 2. The nanoscale B2 particles were seen to be mainly composed by Ni and Al, with the latter element being an impurity of the starting powders. The formation of the B2 phase was predicted by thermodynamic calculations, showing the interest of such approach to predict and explain the developed microstructures in the fusion zone of the joint. During fusion welding, there is an intense mixing of elements within the molten pool. As such, it is possible that the B2 particles are formed due to the local mixing of Ni and Al favoring the formation of this phase in the fusion zone of the joint.

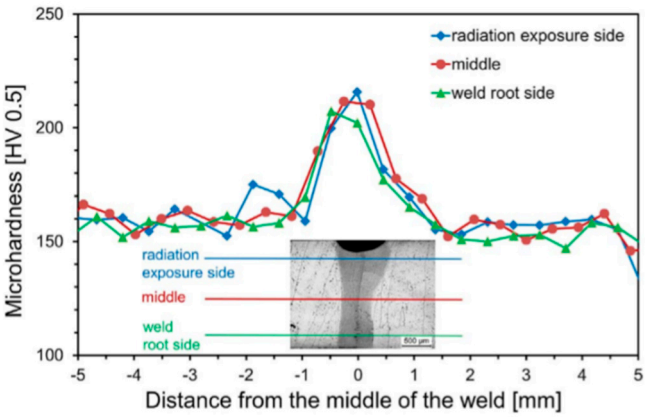

Figure 2. Microhardness profile of a laser beam welded joint (Reproduced from [53], with permission from Elsevier, 2018).

The measured increase of hardness on the welds was suggested by the authors to be an asset for structural applications of this class of HEA. However, no assessement of the tensile properties of the welded joints was performed, thus it was not possible to state the suitabilty of these joints to be employed as structural parts. Though this was not studied in the abovementioned paper, it can be hypothesized that it may be possible to slightly change the microstructure (and resulting properties) in the fusion zone, by controlling the heat input. For example, lower heat input leads to higher cooling rates, which restricts grain growth in the fusion zone of the joint [74].

In a follow-up work, Kashaev et al. [54] addressed the impact of laser welding on the mechanical performance of the welded joints. Due to the coarse grain structure of the base material, with a grain size ranging from 250–500 µm, a refined structure in the fusion zone was observed (100–300 µm). Of special relevance in this work is the fact that the welding process did not impair the mechanical properties of the HEA joints, and the tensile and fatigue behavior of both base material and welded joints were similar (refer to Figure 3). Fracture of the welded joints occurred in the BM, which can be explained by the lower hardness of this region, which promoted strain accumulation.

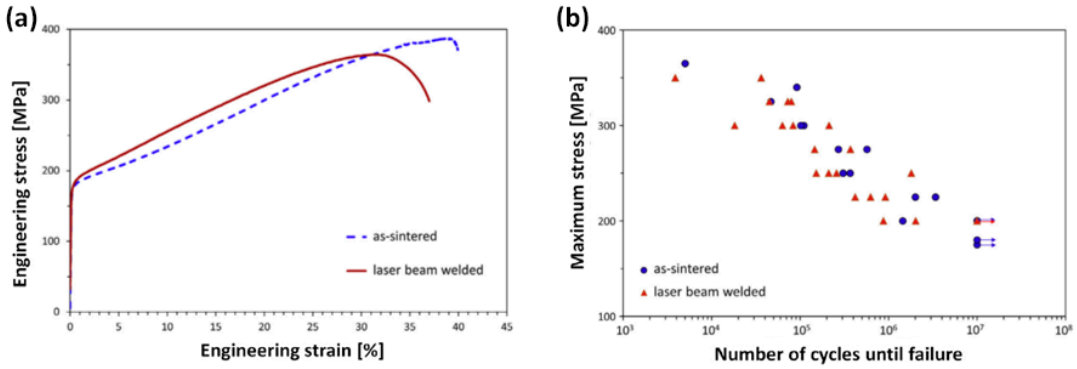

Figure 3. Laser beam welds characterization: (**a**) Tensile testing; (**b**) fatigue testing (Adapted from [54], with permission from Elsevier, 2019).

Other researchers have also used laser welding for similar joining of CoCrFeNiMn HEAs. Jo et al. [55] also found that the hardness of the fusion zone of the joint was higher than in the base materials and also that the FCC structure was preserved. These results show the good reproducibility in terms of mechanical properties in laser welded CoCrFeMnNi HEAs obtained by different research groups. The higher hardness of the fusion zone was attributed to fine dendritic arm spacing and composition inhomogeneity. However, it must be noticed that the BM hardness was that of an as-annealed CoCrFeNiMn HEA [75]. It is known that CoCrFeNiMn alloys can exhibit higher hardness under appropriate heat treatment conditions, which would lead to a lower hardness region in the FZ if the BM was heat treated prior to welding. Obviously, the condition of the BM will impact the microstructural evolution of the welded joints, especially in what concerns strain accumulation upon mechanical testing.

A study on laser welding of as-cast and as-rolled CoCrFeNiMn HEA, was a performed by Nam et al. [56,57] in order to assess their viability for cryogenic applications. On a similar laser welding case, increasing the welding speed, which varied between 6, 8, and 10 m/min, and corresponds to a decrease in the heat input, revealed that the density of shrinkage voids, primary dendrite arm spacing, and dendrite packet size decreased. It should be noted that shrinkage avoids can be avoided/minimized upon careful optimization of the process parameters [76]. The microhardness profiles showed that, on the casted samples, the FZ presented higher values than the BM, which was attributed to the differences in grain size between both regions. Nevertheless, on the as-rolled specimens, no pronounced variation in hardness was observed, due to the existence of similar grain size in both the BM and FZ.

As depicted in Figure 4, the tensile properties of the as-cast specimens were similar to those of the BMs. However, the same did not occur in the as-rolled condition, where the welded region showed lower tensile strength values when compared to the BM, which resulted from the larger grain size on the FZ than in the BM. For the as-cast samples, at a testing temperature of 298 K, fracture occurred near the HAZ/BM interface. The same did not occur on the rolled samples, where fracture occurred in the FZ, which was attributed to higher grain size of this region. Nevertheless, in both cases, the tensile properties of the samples tested at 77 K were superior to those observed as 298 K, which was attributed to the existence of deformation twinning that tends to occur at cryogenic temperatures.

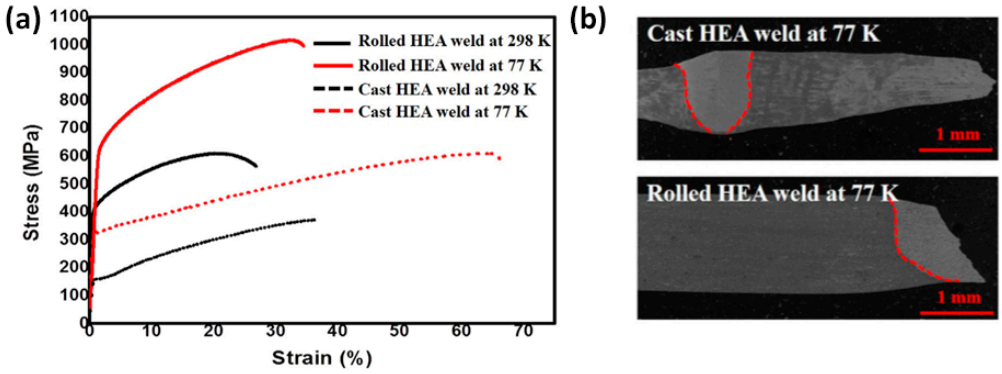

Figure 4. Tensile testing results: (**a**) Comparison between the tensile properties of the weld at different temperatures; (**b**) fracture region (Adapted from [56], with permission from Elsevier, 2019).

In [57], an as-cast and an as-rolled CoCrFeNiMn HEA were welded together, and evident differences of the microstructure were observed between both sides of the joint, as depicted in Figure 5. This phenomenon was attributed to the distinct epitaxial dendritic growth that initiated from the different grain sizes and morphologies in the BMs.

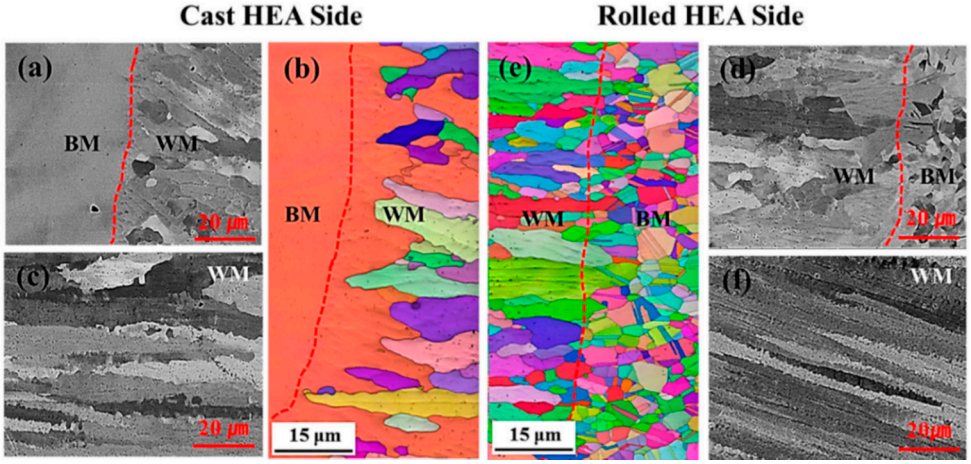

Figure 5. Microstructure of the dissimilar welds: (**a**,**b**) Dendritic growth nucleated from the fusion boundary on the cast HEA (high entropy alloy) side; (**c**) dendrites from near the centerline on the cast WM side; (**d**,**e**) dendritic growth nucleated from the fusion boundary on the rolled HEA side; (**f**) Dendrites from near the centerline on the rolled WM side. BM—Base material; WM—Weld metal (Reproduced from [57], with permission from Taylor & Francis, 2019).

The microhardness increased on the as-cast BM/HAZ interface, but still, no significant change could be observed in the weld/rolled BM interface (refer to Figure 6). Overall, the tensile properties were enhanced when the material was tested in cryogenic conditions due to deformation twinning. During tensile testing, the dissimilar welds fractured on the as-cast BM, exhibiting a comparable

behavior to that of the as-cast alloy. In both cases, the viability of the laser welded CoCrFeNiMn HEAs joints for applications in cryogenic environments was evidenced.

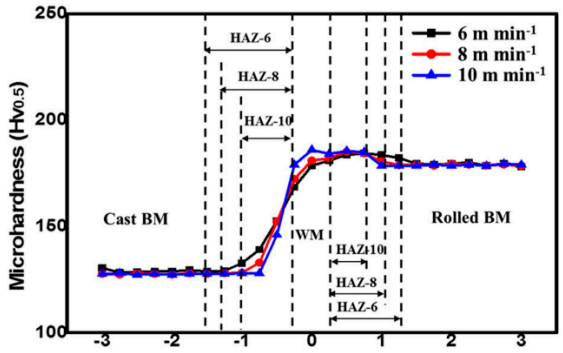

Figure 6. Microhardness profile of the dissimilar weld (Reproduced from [57], with permission from Taylor & Francis, 2019).

In another work on welding of the CoCrFeNiMn system, Chen et al. [58] showed that their laser welded samples had superior properties than that of the BM, since fracture of the joints occurred in that region rather than in the FZ. This could be attributed to the higher hardness of the fusion zone (≈193 HV) when compared to the base material (≈177 HV). The microstructural analysis of the weld region and BM revealed a single FCC phase with several Cr-Mn rich precipitates. In the fusion zone, the average size of the existing precipitates ranged from 0.41 to 0.49 μm, dispersed within the grains and at the grain boundaries. These, owing to their small size, have a pinning effect on dislocations [77], granting the welded region a superior mechanical performance than the BM.

Often, the resultant microstructures in fusion-based welded joints must be modified in order to improve the part mechanical properties. These microstructural modifications are often performed by post-weld heat treatments, which can induce dissolution or formation of new phases/precipitates or promote stress relieving [78–81].

The influence of post-weld heat treatments on laser welded CoCrFeNiMn HEAs was also reported in the literature. Nam et al. [59] studied the effect of post-weld heat treatments on a temperature range of 800 and 1000°C for one hour, on laser beam welds of a cold-rolled CoCrFeNiMn HEA. Before the heat-treatment, the welded region exhibited a larger grain size and inferior tensile strength and hardness than the BM. After being heat-treated, the welds showed superior hardness than the BM, with the FZ preserving the original BM FCC crystal structure and a decrease in the size and fraction of Cr-Mn oxide inclusions. With the increase of temperature of the heat treatment to 1000 °C, the variation in grain size between the weld metal and heat-affected zone decreased, which resulted in approximately the same tensile properties between the welded joint and the BM. This initial work shows the fundamental role of critically selecting the base material initial condition and subsequent post-weld heat treatments. These are fundamental to improve the joint microstructure and consequently its mechanical properties.

Concerning other fusion-based welding techniques, Wu et al. [60,61] investigated Electron Beam Welding and Gas Tungsten Arc Welding (GTAW) on a CoCrFeMnNi HEA. For this purpose, ingots were produced via arc-melting and then thermomechanically processed to achieve a homogeneous equiaxed microstructure. After welding, microstructure characterization evidenced that no major defects existed in the joints, and that the microstructure was mainly composed of dendrites and large columnar grains. Overall, the yield strength of both welded joints was higher than that of the BM. Differences between both welding methods resided on the dendrite arm spacing and on the amount of elemental segregation, which were less evident on the electron beam welds. This can be attributed to the fast cooling rate of the process, which can decrease grain growth and elemental segregation when compared to arc-based techniques [47,48]. The tensile strength of the GTAW samples exhibited, approximately, 80% of the tensile strength and 50% of the ductility of the BM, while the electron

beam-welded samples presented a similar behavior to that of the BM. Though sound joints were achieved in both cases, the ability of electron beam welding to localize the heat in a restrict region can be considered an advantage and a potential justification on the superior mechanical properties when compared to arc-based welding of the same alloy.

More recently, Oliveira et al. [62] performed a comprehensive study on GTAW of as-rolled CoCrFeNiMn HEA. Using synchrotron X-ray diffraction analysis, the authors observed that the extension of the HAZ was larger than that determined based on electron microscopy and hardness measurements techniques. In fact, due to the large deformation imposed by cold rolling of the starting BM, recovery phenomenon was seen to occur far away from the weld centerline. This phenomenon translated into a decrease of the residual stresses of the material in that region, though no variations in grain size and hardness were observed.

The use of filler materials during fusion-based welding is often used to control and adjust the chemical composition and resulting microstructures [82,83]. Moreover, in hard-to-join dissimilar pairs, careful selection of the filler material can aid in the inhibition of solidification cracking or other defects than can occur upon solidification [84,85].

Nam et al. [63] evaluated the use of two different filler materials during similar GTAW of an CoCrFeMnNi HEA. The selected filler materials were a 308 L stainless steel, while the other had the same composition as the BM. The results evidenced that both types of welds exhibited a single FCC phase, nevertheless the elemental percentage of Fe increased with the proximity to the weld centerline when the stainless steel filler was used. Regarding the mechanical properties, both welds exhibited superior values than the original BM. The joint obtained using the CoCrFeMnNi filler presented the higher values for the microhardness (≈165 ± 1 HV), as depicted in Figure 7a. The tensile properties were also assessed at room and cryogenic temperatures, exhibiting a comparable behavior to that of the cast BM, as presented in Figure 7b. Overall, the tensile testing provided an insight for the possibility to use stainless steel 308 L as a filler metal to guarantee the applicability of these HEAs in cryogenic environments.

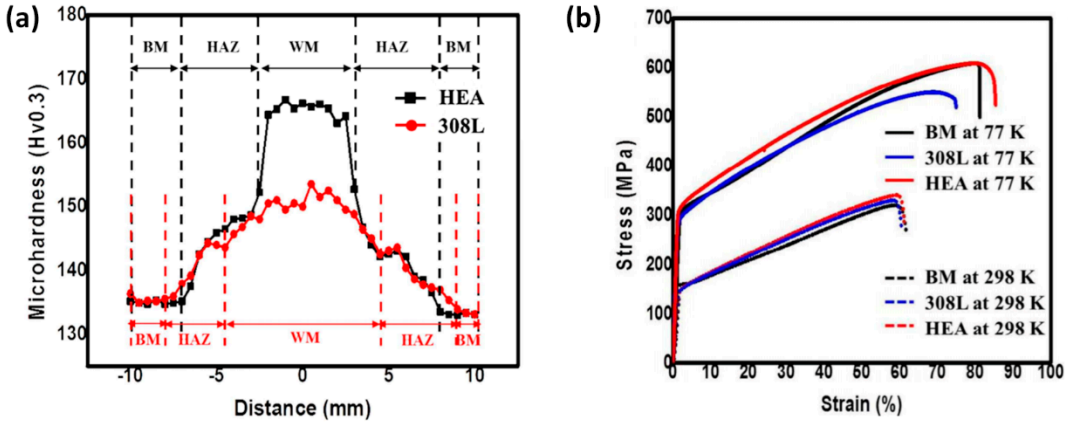

Figure 7. Mechanical behavior of the welded joints: (**a**) Tensile testing; (**b**) microhardness distribution (Adapted from [63], with permission from Elsevier, 2020).

Due to the possibility to control the composition, and therefore the resulting microstructures using filler materials, we hypothesize that in the future, dedicated filler materials can be developed to control and tune the HEA joints properties.

2.1.2. Other HEA Systems

Most of the works on welding of HEAs currently focus on the CoCrFeNiMn system, as exemplified above. However, some researchers started to pay attention to the weldability of other HEA compositions.

The use of GTAW for welding of an $Al_{0.5}$CoCrFeNi HEA was attempted by Sokkalingam et al. [66]. The BM was composed by a near-equiaxed microstructure and, after welding, the HAZ exhibited a microstructure with a size, approximately, double of that of the BM. This is explained by the weld thermal cycle, that is known to induce grain growth in the HAZ, especially closer to the fusion boundary. Additionally, the FZ was characterized by dendritic growth, and near the weld centerline, a fine equiaxed microstructure could be observed. Both the BM and the FZ exhibit a mixed FCC and BCC structure. However, the volumetric fraction of the BCC phase was reduced due to the thermal history experienced by the material during the welding procedure. Mechanical testing showed that the weld region exhibited an inferior microhardness, and the tensile properties experienced a reduction of 6.4% in strength and 16.5% in ductility, when compared to the BM.

The same authors also performed dissimilar welding of $Al_{0.1}$CoCrFeNi HEA to AISI304 stainless steel by GTAW [65]. As depicted in Figure 8, microstructural characterization revealed that the HEA side of the weld was characterized by epitaxial grain growth, while the AISI304 stainless steel side exhibited non-epitaxial grain growth. Nevertheless, towards the weld centerline, the joint tends to exhibit an equiaxed dendritic grain structure. During tensile testing, fracture occurred in the fusion zone, which was attributed to the heterogeneous distribution of the microstructure and lower hardness of the weld. Overall, the applicability of these dissimilar joints for structural applications was confirmed by means of mechanical testing, where the dissimilar joint exhibited superior values for the yield strength and ultimate tensile strength (≈265 and ≈590 MPa, respectively) than that of the HEA side of the BM (≈148 and ≈327 MPa, respectively).

Figure 8. Microstructural characterization by means of EBSD (Electron Backscatter Diffraction) inverse pole figure analysis of the dissimilar welds. BM-1: $Al_{0.1}$CoCrFeNi HEA; BM-2: AISI304 stainless steel (Reproduced from [65] with permission from Cambridge University Press, 2019).

The corrosion behavior of laser welded $Al_{0.5}$CoCrFeNi HEA was studied by Sokkalingam et al. [64], by evaluating the corrosion potential and corrosion current density obtained by potentiodynamic polarization tests. The BM was composed by an equiaxed microstructure composed by Cr-Fe and Al-Ni rich phases and Al-rich particles. During welding, the dissolution of the Al-Ni rich and Al-rich compounds into the CoCrFeNi matrix occurred, resulting in a microstructure exhibiting Cr-Fe rich columnar dendrites with an Al-Ni rich interdendritic region. Overall, the results from the corrosion resistance tests evidenced that the welded joints exhibited a higher corrosion resistance than the BM alone, when exposed to aqueous corrosion environments. This was attributed to the solubility of the Al in the alloy matrix during welding that causes an increase of its corrosion potential, resulting on the reduction of the galvanic circuit in the joint.

More recently, weldability studies on Al_xCoCrCu$_y$FeNi HEAs have been performed by Martin et al. [67,68]. Cu segregation was seen to promote solidification cracking in the fusion zone of the GTAW joints. By changing the alloy composition, it was possible to mitigate the cracking susceptibility of this HEA class. These works, which were supported by thermodynamic calculations to predict the existing phases on the FZ as function of the alloy composition, show the importance of optimizing the BM starting composition when cracking phenomena, such as hot cracking and liquation

cracking, are prone to occur in the materials to be welded. Though this was only observed in the AlCoCrCuFeNi HEA system, it is likely that other HEA compositions may exhibit the problems. If that is the case, the addition of filler materials [48] can also be a potential solution to adjust and improve the chemical composition of the fusion zone.

Panina et al. [69] reported the effects of pre-heating temperature (400, 600, and 800 °C) on the laser weldability of a $Ti_{1.89}NbCrV_{0.56}$ refractory high entropy alloy. Initially, the BM microstructure was mainly composed by BCC grains presenting also small C15 Laves phase particles. Hot cracking occurred when welding was performed with the BM at room temperature and at 400 °C, which was attributed to the low ductility of the alloy. Since during welding thermal stresses are generated, materials with poor ductility can suffer cracking if those stresses are not relieved. Using pre-heating temperatures of 600 °C and 800 °C, however, resulted in defect-free joints. The microstructure of the welds was characterized by columnar grains, where the grain size tended to increase with the increase of pre-heating temperatures. This can be explained based on the effect of changing the pre-heating temperature before welding: Higher pre-heating temperature leads to a slower cooling rate, which promotes more significant grain growth. Due to these slower cooling rates, the grain size was larger in the different FZ. As such, the microhardness of the FZ tended to decrease with the increase of the selected pre-heating temperatures. The mechanical performance of the welds was also assessed through tensile testing at 750 °C, and enhanced tensile properties were observed when pre-heating at 800 °C (ductility of ≈10%, yield strength of 265 MPa and ultimate tensile strength of 285 MPa vs. the 250 MPa maximum stress obtained when fracture occurred in the elastic region on the as-cast specimens). Overall, the results obtained in this study highlight the need for optimizing the welding parameters, such as the pre-heating temperatures, in order to obtain high performing joints.

Currently, it is clear that welding of HEAs is a growing research topic. However, most of the work is focused on the CoCrFeNiMn alloy system using high power beams (laser and electron beam). Though some recent studies have addressed the weldability of other HEA systems, the existence of a significant research gap regarding the weldability of these materials is highly noticeable.

2.2. Solid-State Welding of HEAs

As previously mentioned, welding materials in the solid state can be a reliable and advantageous way to achieve sound joints. The current information regarding welding HEAs using solid-state techniques shows that most studies are focused on friction stir welding (FSW) [55,86–92]. Nevertheless, other possibilities for joining these materials are rotary friction welding [91] and diffusion bonding [92].

Concerning FSW, the literature shows that an effort for the development and comprehension of the microstructural evolution of FSWed HEAs joints is underway. For instance, FSW of a CoCrFeNiMn HEA manufactured by vacuum induction melting, followed by thermomechanical processing was conducted by Jo et al. [55]. After the welding process, the tensile strength and the ductility of the samples exhibited a similar behavior to that of the BM. Ductile fracture occurred in the BM, indicating that the microstructure evolution in the processed region promoted a higher joint strength. The welding process was characterized by inducing dynamic recrystallization, which resulted in grain refinement aided by the temperature increase, coupled with the massive deformation imposed during the process. The microhardness distribution on the welds exhibited higher values than the BM. An EBSD (Electron Backscatter Diffraction) inverse pole analysis on the cross section of the weld exhibited significant grain refinement and a lower proportion of twins at the center of the weld, indicating also that the fraction of low angle grain boundaries tends to decrease with the increase of distance from the weld center. These boundaries have an important role on the mechanical performance of the material acting as barriers to plastic deformation and inhibiting the grain growth mechanisms induced by the increase of temperature.

Typically, it is often preferred that failure of a welded joint occurs in the BM. This is an evidence of the higher resistance of the welded region, which implies that, for structural parts, the main limiting aspect will be the BM mechanical properties. Provided that those properties are ensured to be constant

over time, and since FSW is known to be a very reliable process, unlike some arc-based welding processes, the welded joints can be safely used as structural parts in key engineering applications.

A step further into the investigation of the FSW process applied to the CoCrFeNiMn HEA was taken by Xu et al. [86]. In this work, forced cooling was applied to the processed material, aiming at improving the joint properties. The mechanical results showed that it is possible to enhance the mechanical properties of the welds without a ductility loss through the fast cooling of the joint. This enhancement of the material mechanical properties was explained by the inhibition of the static recovery and selected grain growth that can occur during post-annealing.

Zhu et al. [87] performed FSW on cast $CoCrFeNiAl_{0.3}$. Defect-free welds were obtained using two different speeds, 30 and 50 mm/min. In both cases, apart from the original FCC matrix, the results from X-ray diffraction analysis showed that no phase changes occurred. The morphology of the welds exhibited four typical thermomechanically affected areas after FSW: (i) SZ, the stir zone, where refined equiaxed grains resultant from recrystallization were observed; (ii) TMAZ, the thermomechanically affected zone, which exhibited both coarse and fine grains; (iii) HAZ, where columnar grains were observed with an average size of 132 µm; (iv) BM, characterized by columnar grains resultant from the casting process, preferentially oriented in the solidification direction. Because of these microstructural differences, the microhardness was higher at the center of the weld, decreasing with the distance from the center. Additionally, reducing the speed of the tool, which increases the heat input, resulted in slightly a larger grain size on the SZ, which is in good agreement with the effect of FSW process parameters on other materials [93].

In another study, Zhu et al. [88] studied a quaternary HEA composition, $Co_{16}Cr_{28}Fe_{28}Ni_{28}$, in order to study the effects of the reduced Co content on the material mechanical performance. Their work showed that after recrystallization, through thermomechanical processing, the tensile properties were superior to that of common HEAs, as depicted in Figure 9a. Such evidenced the possibility for the enhancement of the alloy mechanical properties through precipitation hardening, given the reduced proportion of Co. By performing FSW on this HEA, varying only the welding speed (ranging between 30 and 50 mm/min), a refined microstructure composed of equiaxed grains was obtained in the SZ, which remained with its original FCC crystal structure. However, at the higher level of welding speed, the formation of a kissing bond [94], which is characterized by the partial penetration of the weld, was inevitable, due to low heat input. In both cases, the formation of a white band was evidenced. Further analysis of this feature revealed the presence of W-rich and Cr-rich particles. The presence of W-rich particles can be explained by the welding tool wear, which is a common occurrence during FSW [95]. The presence of the Cr-rich particles was not explained, requiring further experimental work to justify its presence. Regarding the hardness of the joints, the SZ exhibited a relatively higher hardness than the BM, which was attributed to the distorted crystalline network, high fraction of deformation twins, and refined grain structure (see Figure 9b regarding the hardness profile obtained across the joint).

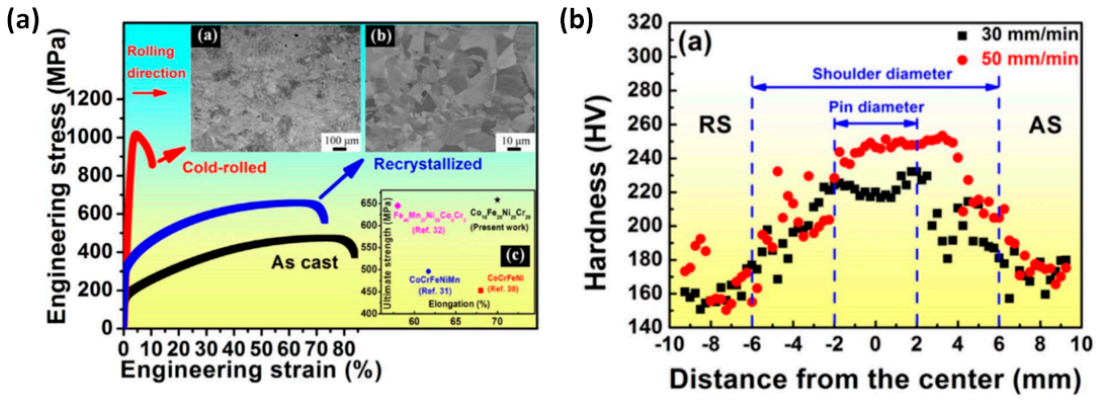

Figure 9. Sample characterization: (**a**) Tensile properties; (**b**) microhardness distribution (Adapted from [88], with permission from Elsevier, 2018).

During FSW, tool wear can occur, and debris can be incorporated in the processed material. The influence of tungsten and chromium carbide particles, caused by the tool deterioration during FSW of a CoCrFeNiMn HEA was accessed by Park et al. [89]. The process parameters comprised a welding speed of 30 mm/min, while the tool rotation varied between 400, 600, 800, and 1000 rpm. The results showed that both the welds and the BM exhibited a single FCC crystal structure. No cracks or voids were found on the welds, although the increase of tool rotation resulted in thinning near the center line, which corresponds to an inferior thickness of the weld when compared to the BM. The formation of a tornado-shaped region on the SZ was also evidenced when performing FSW with rotations speeds higher than 600 rpm (refer to Figure 10a). This tornado-shaped region was characterized by the formation of a secondary phase correspondent to W- and Cr-rich carbides, aided by the tool wear. Overall, superior characteristics regarding the hardness, tensile strength, and joint efficiency were obtained with a rotation speed of 800 rpm, where the grain size was at its lowest value. This was attributed to the different heat inputs that govern the solid-state transformation during the process. As depicted in Figure 10b, a comparison on the carbide size and concentration can be observed between a lower heat input (800 rpm) and a higher heat input sample (1000 rpm). These results show that higher rotation speeds lead to more severe wear of the FSW tool.

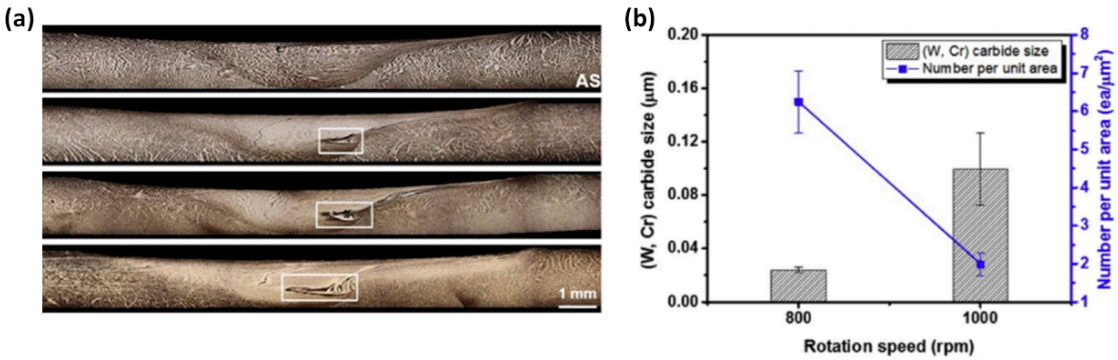

Figure 10. Characterization of friction stir welded (FSWed) CoCrFeNiMn joints: (**a**) Morphology of the welds at different rotation speeds (from top to bottom: 400, 600, 800, 1000 rpm); (**b**) carbide content at 800 rpm and 1000 rpm (Adapted from [89], with permission from Elsevier, 2019).

On another perspective, Shaysultanov et al. [90] performed FSW on a carbon-doped CoCrFeNiMn HEA, with the intent of studying the influence this controlled C addition on the welded joints mechanical performance. After being produced via thermite-type self-propagating high-temperature synthesis, the samples were cold-rolled and annealed at 900 °C for 1 h, to obtain an equiaxed microstructure. The welds resultant from the FSW process were defect-free, while microstructural differences were observed on the grain size on the BM and the SZ, with a change from 9.2 to 4.6 μm, respectively. With this joining process the proportion of $M_{23}C_6$ carbides increased, which was attributed to the rise in temperature triggered by intense plastic deformation, aiding in the precipitation of this phase. Overall, the mechanical performance of the welds exhibited higher values than the BM in both the microhardness (an increase of ≈40 HV) and tensile properties (an increase of ≈80 MPa on the ultimate tensile strength and of ≈200 MPa on the yield strength), which can be attributed to the carbides' precipitation.

As described above, most of the research work on solid-state welding of HEA focuses on FSW. However, other solid-state techniques have also started to be used to join this class of advanced materials.

Rotary friction welding was conducted in a eutectic $AlCoCrFeNi_{2.1}$ HEA by Li et al. [91]. As depicted in Figure 11a–c, similarly shaped joints were obtained with friction pressures of 80 and 120 MPa, while welding at 200 MPa resulted in an increase of the burn-off length and on the size of the resulting flash. Microstructurally, at the center of the weld, on the dynamic recrystallization zone (DRZ), the grains exhibited a refined and equiaxed structure. Additionally, on the TMAZ, the microstructure is composed of bent and elongated grains, while the HAZ exhibited fewer eutectic cells when compared

to the BM. An EBSD analysis of the samples produced under the friction pressure of 120 MPa, revealed both an FCC phase, composed mainly by Fe, Co, and Cr, and a B2 phase, composed of AlNi intermetallic compounds and BCC structured-type CrFe precipitates. The tensile properties were superior when the friction pressure was of 200 MPa, where fracture of the joints occurred in the BM. As depicted in Figure 11d–f, the rough fractured surface is the result of the diferent ductility of the hard B2 phase and the soft FCC phase. Nevertheless, the specimens welded with 80 and 120 MPa of friction pressure yielded inferior tensile performance, fracturing at the joint interface, which is due to the the existence of a weld interface and discontinuous distribuition of the B2 phase on the DRZ region.

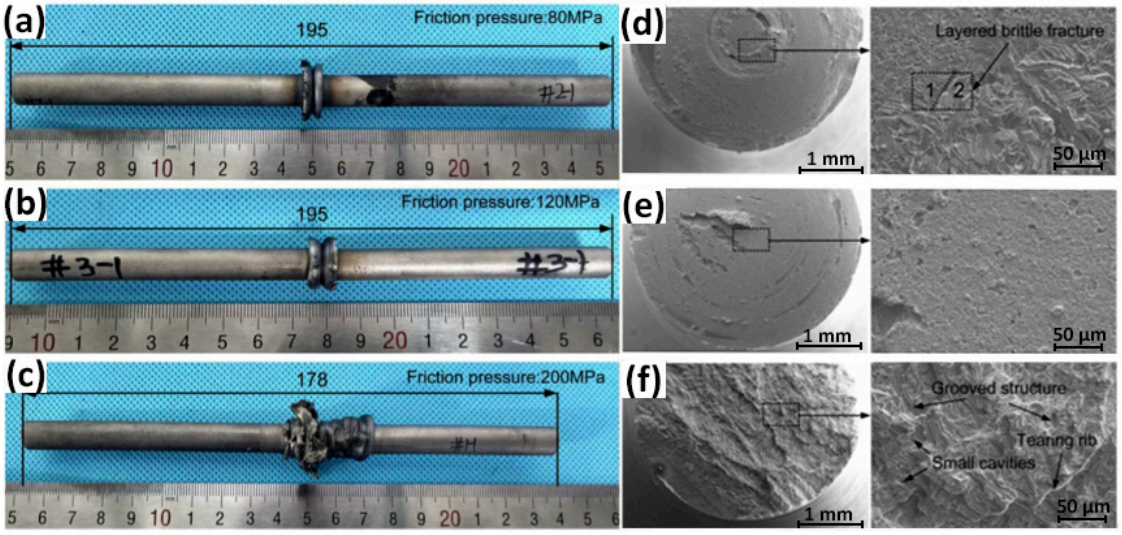

Figure 11. Morphology of the welds and fractured surfaces after tensile testing. The joints were obtained under the friction pressures of: (**a**) and (**d**) 80 MPa; (**b**) and (**e**) 120 MPa; (**c**) and (**f**) 200 MPa (Adapted from [91], with permission from Elsevier, 2020).

Another possibility for welding materials in the solid state is through diffusion bonding. Unlike other solid-state welding processes, this technique proves its purpose when joining materials with a high susceptibility to cracking, as in the case of refractory metals [96–98]. Lei et al. [92] studied vacuum diffusion bonding between the single-phase FCC $Al_{0.85}CoCrFeNi$ HEA and a TiAl alloy. For this purpose, an axial pressure of 30 MPa, a temperature range of 750 to 1050 °C, and a holding time of 30 to 120 min were used. Given the sluggish diffusion effect, characteristic of HEA systems, the atomic diffusion from the TiAl substrate into the HEA substrate was drastically inferior, when compared to the diffusion resultant from the HEA side. As depicted in Figure 12, the obtained bonds were characterized by having three distinct regions, which could be divided according with their microstructural composition: Region I, composed by α_2-Ti_3Al + solid strengthened γ-TiAl; region II, which can be expressed as $Al(Co, Ni)_2Ti$; and region III, characterized by an Cr(Fe, Co) solid solution phase. The formation of voids was noticeable in the interlayer between regions II and III, which was caused by the atomic flux imbalance provided by the process parameters in use. Overall, the optimal results yielded a maximum microhardness of 923 HV in region I, and a maximum shear strength of 71 MPa (at 850 °C and after 90 min of holding time).

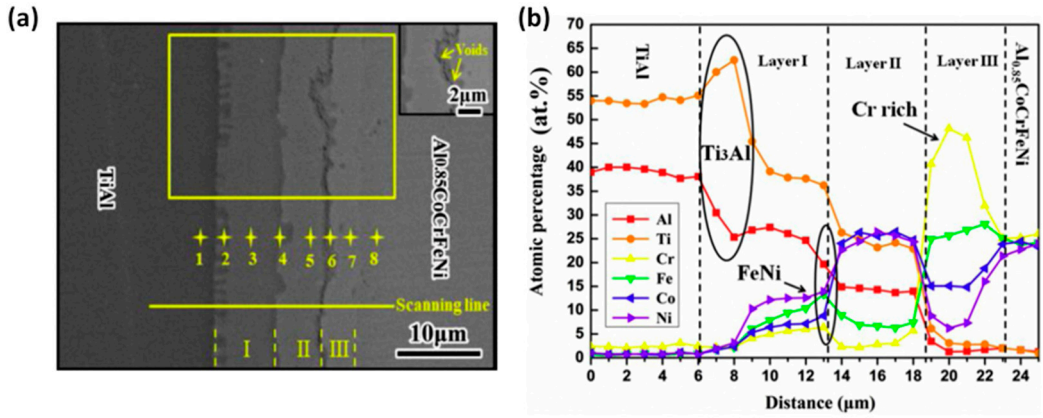

Figure 12. Characterization of the diffusion bonded TiAl/Al0.85CoCrFeNi joints using 950 °C/1 h/30 MPa: (**a**) microstructure under SEM; (**b**) Compositional element distribution taken from the scanning line region (Adapted from [92], with permission from Elsevier, 2020).

As it can be inferred from this work, multiple welding works on HEA currently exist, and increasing attention to these alloys' weldability is emerging. Table 2 compiles the existing studies on welding of different HEA, while Figure 13 details the relative importance of each welding technique already applied to HEAs. As it can be noted, most studies concern the CoCrFeNiMn HEA, showing the need to further extend these research works to other alloys systems.

Table 2. Summary of the welding techniques currently used on HEAs.

Welding Technique	Alloy System	Refs.
Brazing	CoCrFeNiMn CoCrFeNi	[52]
Laser Welding	CoCrFeNiMn TiNbCrV	[53–59] [69]
Gas Tungsten Arc Welding	AlCoCrFeNi AlCoCrCuFeNi CoCrFeNiMn	[64–66] [67,68] [61–63]
Electron Beam Welding	CoCrFeNiMn	[60,61]
Friction Stir Welding	CoCrFeNiMn AlCoCrFeNi CoCrFeNi	[55,86,89,90] [87] [88]
Rotary Friction Welding	AlCoCrFeNi	[91]
Diffusion Bonding	AlCoCrFeNi	[92]

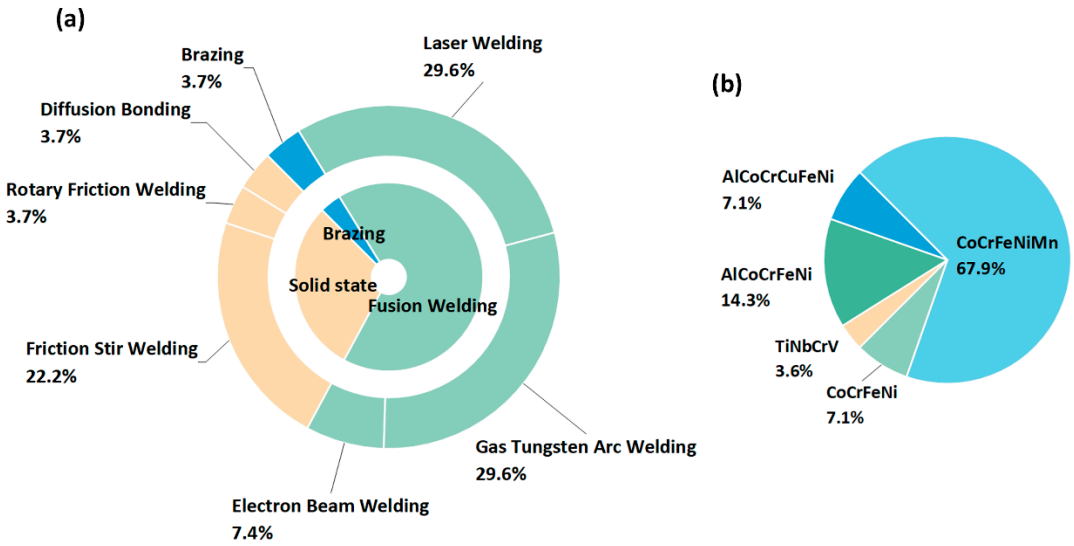

Figure 13. Percentage distribution of the number of papers considered in this study: (**a**) by welding technique; (**b**) by alloy system.

3. Summary and Conclusions

The present article offers an overview on the current status and progress on welding of high entropy alloys. The literature reveals that the main developments on this topic are mainly focused on fusion-based process by means of laser welding, whereas solid-state ones focus on being put on friction stir welding. Nevertheless, it is highly noticeable that the improvement of the welding processes regarding the feasibility of structural and functional applications of HEAs is at its beginning stage.

Regarding fusion-based processes, the current developments show that a step towards the optimization of laser-based methods is being taken. Nevertheless, a need for research on the joining of HEAs through other fusion-based techniques, that are economically more viable than laser-based approaches, is of great interest. Additionally, beyond the welding process, the initial condition of the alloy affects the weld microstructure and its behavior. Such a matter is important to study the four core effects characteristic of HEAs and their impact on the microstructural transformations on the molten pool and mechanical performance of the welds.

Concerning solid-state processes, the literature shows that success on joining CoCrFeNiMn HEAs has been achieved, although there is still a need for the optimization of the process parameters to accomplish high performing joints. Regarding their mechanical behavior, the joints show good mechanical properties, although there is still a need to enhance such solid-state processes into what that makes HEAs competitive, e.g., their outstanding behavior in extreme conditions.

Currently, special emphasis is being put on the most studied CoCrFeNiMn system. However, to further expand the potential applications of HEAs, other alloy systems need to be explored. No major work on dissimilar joints exists yet. This is another key area of interest where the need to couple the properties of different materials is of great interest.

Currently, it is well-known that HEAs can incorporate impurities during their casting. These impurities can lead to the formation on unexpected phases, especially under the non-equilibrium solidification of fusion-based processes. These unexpected phases were already observed for the CoCrFeMnNi system, and were seen to improve the joint mechanical properties. However, it is not necessarily true that these impurities will always be beneficial for the joint microstructure and performance, and as such, efforts should be made to improve the chemical homogeneity of the starting BMs, but also address the potential formation of these phases and propose methods to mitigate them.

All in all, the future of welding of HEA is at its early stages with the potential to further expand the potential applications of these advanced engineering materials.

Author Contributions: Both authors contributed equally to the research of the literature and writing of the review paper. All authors have read and agreed to the published version of the manuscript.

Funding: This research was funded by Fundação para a Ciência e a Tecnologia (FCT - MCTES) via the project UIDB/00667/2020 (UNIDEMI).

Acknowledgments: JGL and JPO acknowledge Fundação para a Ciência e a Tecnologia (FCT - MCTES) for its financial support via the project UIDB/00667/2020 (UNIDEMI).

Conflicts of Interest: The authors declare no conflict of interest.

References

1. Cantor, B.; Chang, I.T.H.; Knight, P.; Vincent, A.J.B. Microstructural development in equiatomic multicomponent alloys. *Mater. Sci. Eng. A* **2004**, *375–377*, 213–218. [CrossRef]
2. Yeh, J.W.; Chen, S.K.; Lin, S.J.; Gan, J.Y.; Chin, T.S.; Shun, T.T.; Tsau, C.H.; Chang, S.Y. Nanostructured high-entropy alloys with multiple principal elements: Novel alloy design concepts and outcomes. *Adv. Eng. Mater.* **2004**, *6*, 299–303. [CrossRef]
3. Miracle, D.B.; Senkov, O.N. A critical review of high entropy alloys and related concepts. *Acta Mater.* **2017**, *122*, 448–511. [CrossRef]
4. Gao, M.C.; Liaw, P.K.; Yeh, J.W.; Zhang, Y. *High.-Entropy Alloys: Fundamentals and Applications*; Springer International Publishing: Cham, Switzerland, 2016; ISBN 9783319270135.
5. Zhang, Y.; Zuo, T.T.; Tang, Z.; Gao, M.C.; Dahmen, K.A.; Liaw, P.K.; Lu, Z.P. Microstructures and properties of high-entropy alloys. *Prog. Mater Sci.* **2014**, *61*, 1–93. [CrossRef]
6. Murty, B.S.; Yeh, J.W.; Ranganathan, S.; Bhattacharjee, P.P. *High-Entropy Alloys*, 2nd ed.; Elsevier: Amsterdam, The Netherlands, 2019; ISBN 9780128160671.
7. Ikeda, Y.; Grabowski, B.; Körmann, F. Ab initio phase stabilities and mechanical properties of multicomponent alloys: A comprehensive review for high entropy alloys and compositionally complex alloys. *Mater. Charact.* **2019**, *147*, 464–511. [CrossRef]
8. Li, W.; Liaw, P.K.; Gao, Y. Fracture resistance of high entropy alloys: A review. *Intermetallics* **2018**, *99*, 69–83. [CrossRef]
9. Li, Z.; Zhao, S.; Ritchie, R.O.; Meyers, M.A. Mechanical properties of high-entropy alloys with emphasis on face-centered cubic alloys. *Prog. Mater Sci.* **2019**, *102*, 296–345. [CrossRef]
10. Chen, J.; Zhou, X.; Wang, W.; Liu, B.; Lv, Y.; Yang, W.; Xu, D.; Liu, Y. A review on fundamental of high entropy alloys with promising high–temperature properties. *J. Alloys Compd.* **2018**, *760*, 15–30. [CrossRef]
11. Couzinié, J.P.; Dirras, G. Body-centered cubic high-entropy alloys: From processing to underlying deformation mechanisms. *Mater. Charact.* **2019**, *147*, 533–544. [CrossRef]
12. George, E.P.; Curtin, W.A.; Tasan, C.C. High entropy alloys: A focused review of mechanical properties and deformation mechanisms. *Acta Mater.* **2019**. [CrossRef]
13. Shi, Y.; Yang, B.; Liaw, P.K. Corrosion-Resistant High-Entropy Alloys: A Review. *Metals* **2017**, *7*, 43. [CrossRef]
14. George, E.P.; Raabe, D.; Ritchie, R.O. High-entropy alloys. *Nat. Rev. Mater.* **2019**, *4*, 515–534. [CrossRef]
15. Tsai, M.-H.; Yeh, J.-W. High-Entropy Alloys: A Critical Review. *Mater. Res. Lett.* **2014**, *2*, 107–123. [CrossRef]
16. Senkov, O.N.; Miracle, D.B.; Chaput, K.J.; Couzinie, J.-P. Development and exploration of refractory high entropy alloys—A review. *J. Mater. Res.* **2018**, *33*, 3092–3128. [CrossRef]
17. Zhang, W.; Liaw, P.K.; Zhang, Y. Science and technology in high-entropy alloys. *Sci. China Mater.* **2018**, *61*, 2–22. [CrossRef]
18. Yeh, J.W. Recent progress in high-entropy alloys. *Ann. Chim. Sci. Mat.* **2006**, *31*, 633–648. [CrossRef]
19. Ng, C.; Guo, S.; Luan, J.; Shi, S.; Liu, C.T. Entropy-driven phase stability and slow diffusion kinetics in an $Al_{0.5}$CoCrCuFeNi high entropy alloy. *Intermetallics* **2012**, *31*, 165–172. [CrossRef]
20. Wu, Y.D.; Cai, Y.H.; Chen, X.H.; Wang, T.; Si, J.J.; Wang, L.; Wang, Y.D.; Hui, X.D. Phase composition and solid solution strengthening effect in TiZrNbMoV high-entropy alloys. *Mater. Des.* **2015**, *83*, 651–660. [CrossRef]
21. He, Q.; Yang, Y. On Lattice Distortion in High Entropy Alloys. *Front. Mater.* **2018**, *5*. [CrossRef]
22. Pickering, E.J.; Muñoz-Moreno, R.; Stone, H.J.; Jones, N.G. Precipitation in the equiatomic high-entropy alloy CrMnFeCoNi. *Scr. Mater.* **2016**, *113*, 106–109. [CrossRef]

23. Bhattacharjee, P.P.; Sathiaraj, G.D.; Zaid, M.; Gatti, J.R.; Lee, C.; Tsai, C.-W.; Yeh, J.-W. Microstructure and texture evolution during annealing of equiatomic CoCrFeMnNi high-entropy alloy. *J. Alloys Compd.* **2014**, *587*, 544–552. [CrossRef]
24. Dąbrowa, J.; Zajusz, M.; Kucza, W.; Cieślak, G.; Berent, K.; Czeppe, T.; Kulik, T.; Danielewski, M. Demystifying the sluggish diffusion effect in high entropy alloys. *J. Alloys Compd.* **2019**, *783*, 193–207. [CrossRef]
25. Nene, S.S.; Frank, M.; Liu, K.; Sinha, S.; Mishra, R.S.; McWilliams, B.A.; Cho, K.C. Corrosion-resistant high entropy alloy with high strength and ductility. *Scr. Mater.* **2019**, *166*, 168–172. [CrossRef]
26. Pathak, S.; Kumar, N.; Mishra, R.S.; De, P.S. Aqueous Corrosion Behavior of Cast CoCrFeMnNi Alloy. *J. Mater. Eng. Perform.* **2019**, *28*, 5970–5977. [CrossRef]
27. Shang, C.; Axinte, E.; Sun, J.; Li, X.; Li, P.; Du, J.; Qiao, P.; Wang, Y. CoCrFeNi($W_{1-x}Mo_x$) high-entropy alloy coatings with excellent mechanical properties and corrosion resistance prepared by mechanical alloying and hot pressing sintering. *Mater. Des.* **2017**, *117*, 193–202. [CrossRef]
28. Shi, Y.; Yang, B.; Xie, X.; Brechtl, J.; Dahmen, K.A.; Liaw, P.K. Corrosion of Al xCoCrFeNi high-entropy alloys: Al-content and potential scan-rate dependent pitting behavior. *Corros. Sci.* **2017**, *119*, 33–45. [CrossRef]
29. Shukla, S.; Wang, T.; Cotton, S.; Mishra, R.S. Hierarchical microstructure for improved fatigue properties in a eutectic high entropy alloy. *Scr. Mater.* **2018**, *156*, 105–109. [CrossRef]
30. Huo, W.; Fang, F.; Liu, X.; Tan, S.; Xie, Z.; Jiang, J. Fatigue resistance of nanotwinned high-entropy alloy films. *Mater. Sci. Eng. A* **2019**, *739*, 26–30. [CrossRef]
31. Wu, J.M.; Lin, S.J.; Yeh, J.W.; Chen, S.K.; Huang, Y.S.; Chen, H.C. Adhesive wear behavior of Al_xCoCrCuFeNi high-entropy alloys as a function of aluminum content. *Wear* **2006**, *261*, 513–519. [CrossRef]
32. Kong, D.; Guo, J.; Liu, R.; Zhang, X.; Song, Y.; Li, Z.; Guo, F.; Xing, X.; Xu, Y.; Wang, W. Effect of remelting and annealing on the wear resistance of $AlCoCrFeNiTi_{0.5}$ high entropy alloys. *Intermetallics* **2019**, *114*. [CrossRef]
33. Yang, S.; Liu, Z.; Pi, J. Microstructure and wear behavior of the AlCrFeCoNi high-entropy alloy fabricated by additive manufacturing. *Mater. Lett.* **2019**, 127004. [CrossRef]
34. Joseph, J.; Haghdadi, N.; Shamlaye, K.; Hodgson, P.; Barnett, M.; Fabijanic, D. The sliding wear behaviour of CoCrFeMnNi and Al_xCoCrFeNi high entropy alloys at elevated temperatures. *Wear* **2019**, *428–429*, 32–44. [CrossRef]
35. Fang, Y.; Chen, N.; Du, G.; Zhang, M.; Zhao, X.; Cheng, H.; Wu, J. High-temperature oxidation resistance, mechanical and wear resistance properties of Ti(C,N)-based cermets with Al0.3CoCrFeNi high-entropy alloy as a metal binder. *J. Alloys Compd.* **2020**, *815*, 152486. [CrossRef]
36. Klimova, M.V.; Semenyuk, A.O.; Shaysultanov, D.G.; Salishchev, G.A.; Zherebtsov, S.V.; Stepanov, N.D. Effect of carbon on cryogenic tensile behavior of CoCrFeMnNi-type high entropy alloys. *J. Alloys Compd.* **2019**, *811*, 152000. [CrossRef]
37. Jo, Y.H.; Doh, K.Y.; Kim, D.G.; Lee, K.; Kim, D.W.; Sung, H.; Sohn, S.S.; Lee, D.; Kim, H.S.; Lee, B.J.; et al. Cryogenic-temperature fracture toughness analysis of non-equi-atomic $V_{10}Cr_{10}Fe_{45}Co_{20}Ni_{15}$ high-entropy alloy. *J. Alloys Compd.* **2019**, *809*. [CrossRef]
38. He, Z.F.; Jia, N.; Ma, D.; Yan, H.L.; Li, Z.M.; Raabe, D. Joint contribution of transformation and twinning to the high strength-ductility combination of a FeMnCoCr high entropy alloy at cryogenic temperatures. *Mater. Sci. Eng. A* **2019**, *759*, 437–447. [CrossRef]
39. Yeh, J.W.; Lin, S.J. Breakthrough applications of high-entropy materials. *J. Mater. Res.* **2018**, *33*, 3129–3137. [CrossRef]
40. Miracle, D.B.; Miller, J.D.; Senkov, O.N.; Woodward, C.; Uchic, M.D.; Tiley, J. Exploration and Development of High Entropy Alloys for Structural Applications. *Entropy* **2014**, *16*, 494–525. [CrossRef]
41. Miracle, D.B. Critical Assessment 14: High entropy alloys and their development as structural materials. *Mater. Sci. Technol.* **2015**, *31*, 1142–1147. [CrossRef]
42. Gludovatz, B.; Hohenwarter, A.; Catoor, D.; Chang, E.H.; George, E.P.; Ritchie, R.O. A fracture-resistant high-entropy alloy for cryogenic applications. *Science* **2014**, *345*, 1153–1158. [CrossRef]
43. Stepanov, N.D.; Shaysultanov, D.G.; Tikhonovsky, M.A.; Zherebtsov, S.V. Structure and high temperature mechanical properties of novel non-equiatomic Fe-(Co, Mn)-Cr-Ni-Al-(Ti) high entropy alloys. *Intermetallics* **2018**, *102*, 140–151. [CrossRef]
44. Wang, M.; Ma, Z.; Xu, Z.; Cheng, X. Microstructures and mechanical properties of HfNbTaTiZrW and HfNbTaTiZrMoW refractory high-entropy alloys. *J. Alloys Compd.* **2019**, *803*, 778–785. [CrossRef]

45. Senkov, O.N.; Scott, J.M.; Senkova, S.V.; Meisenkothen, F.; Miracle, D.B.; Woodward, C.F. Microstructure and elevated temperature properties of a refractory TaNbHfZrTi alloy. *J. Mater. Sci.* **2012**, *47*, 4062–4074. [CrossRef]
46. Senkov, O.N.; Wilks, G.B.; Scott, J.M.; Miracle, D.B. Mechanical properties of $Nb_{25}Mo_{25}Ta_{25}W_{25}$ and $V_{20}Nb_{20}Mo_{20}Ta_{20}W_{20}$ refractory high entropy alloys. *Intermetallics* **2011**, *19*, 698–706. [CrossRef]
47. Oliveira, J.P.; Miranda, R.M.; Braz Fernandes, F.M. Welding and Joining of NiTi Shape Memory Alloys: A Review. *Prog. Mater Sci.* **2017**, *88*, 412–466. [CrossRef]
48. Oliveira, J.P.; Santos, T.G.; Miranda, R.M. Revisiting fundamental welding concepts to improve additive manufacturing: From theory to practice. *Prog. Mater Sci.* **2019**, *107*, 100590. [CrossRef]
49. Oliveira, J.P.; Ponder, K.; Brizes, E.; Abke, T.; Ramirez, A.J.; Edwards, P. Combining resistance spot welding and friction element welding for dissimilar joining of aluminum to high strength steels. *J. Mater. Process. Technol.* **2019**, *273*, 116192. [CrossRef]
50. Nandan, R.; Debroy, T.; Bhadeshia, H.K.D.H. Recent advances in friction-stir welding—Process, weldment structure and properties. *Prog. Mater Sci.* **2008**, *53*, 980–1023. [CrossRef]
51. Guo, J.; Tang, C.; Rothwell, G.; Li, L.; Wang, Y.-C.; Yang, Q.; Ren, X. Welding of High Entropy Alloys—A Review. *Entropy* **2019**, *21*, 431. [CrossRef]
52. Lin, C.; Shiue, R.K.; Wu, S.K.; Lin, Y.S. Dissimilar infrared brazing of CoCrFe(Mn)Ni equiatomic high entropy alloys and 316 stainless steel. *Crystals* **2019**, *9*, 518. [CrossRef]
53. Kashaev, N.; Ventzke, V.; Stepanov, N.; Shaysultanov, D.; Sanin, V.; Zherebtsov, S. Laser beam welding of a CoCrFeNiMn-type high entropy alloy produced by self-propagating high-temperature synthesis. *Intermetallics* **2018**, *96*, 63–71. [CrossRef]
54. Kashaev, N.; Ventzke, V.; Petrov, N.; Horstmann, M.; Zherebtsov, S.; Shaysultanov, D.; Sanin, V.; Stepanov, N. Fatigue behaviour of a laser beam welded CoCrFeNiMn-type high entropy alloy. *Mater. Sci. Eng. A* **2019**, *766*, 138358. [CrossRef]
55. Jo, M.G.; Kim, H.J.; Kang, M.; Madakashira, P.P.; Park, E.S.; Suh, J.Y.; Kim, D.I.; Hong, S.T.; Han, H.N. Microstructure and mechanical properties of friction stir welded and laser welded high entropy alloy CrMnFeCoNi. *Met. Mater. Int.* **2018**, *24*, 73–83. [CrossRef]
56. Nam, H.; Park, C.; Moon, J.; Na, Y.; Kim, H.; Kang, N. Laser weldability of cast and rolled high-entropy alloys for cryogenic applications. *Mater. Sci. Eng. A* **2019**, *742*, 224–230. [CrossRef]
57. Nam, H.; Park, S.; Chun, E.; Kim, H. Laser dissimilar weldability of cast and rolled CoCrFeMnNi high-entropy alloys for cryogenic applications. *Sci. Technol. Weld. Joining* **2020**, *25*, 127–134. [CrossRef]
58. Chen, Z.; Wang, B.; Duan, B.; Zhang, X. Mechanical properties and microstructure of laser welded FeCoNiCrMn high-entropy alloy. *Mater. Lett.* **2019**, *262*, 127060. [CrossRef]
59. Nam, H.; Park, C.; Kim, C.; Kim, H.; Kang, N. Effect of post weld heat treatment on weldability of high entropy alloy welds. *Sci. Technol. Weld. Joining* **2018**, *23*, 420–427. [CrossRef]
60. Wu, Z.; David, S.A.A.; Feng, Z.; Bei, H. Weldability of a high entropy CrMnFeCoNi alloy. *Scr. Mater.* **2016**, *124*, 81–85. [CrossRef]
61. Wu, Z.; David, S.A.; Leonard, D.N.; Feng, Z.; Bei, H. Microstructures and mechanical properties of a welded CoCrFeMnNi high-entropy alloy. *Sci. Technol. Weld. Joining* **2018**, *23*, 585–595. [CrossRef]
62. Oliveira, J.P.; Curado, T.M.; Zeng, Z.; Lopes, J.G.; Rossinyol, E.; Park, J.M.; Schell, N.; Fernandes, F.M.B.; Kim, H.S. Gas tungsten arc welding of as-rolled CrMnFeCoNi high entropy alloy. *Mater. Des.* **2020**, *189*, 108505. [CrossRef]
63. Nam, H.; Park, S.; Park, N.; Na, Y.; Kim, H.; Yoo, S.-J.; Moon, Y.-H.; Kang, N. Weldability of cast CoCrFeMnNi high-entropy alloys using various filler metals for cryogenic applications. *J. Alloys Compd.* **2020**, *819*, 153278. [CrossRef]
64. Sokkalingam, R.; Sivaprasad, K.; Duraiselvam, M.; Muthupandi, V.; Prashanth, K.G. Novel welding of Al0.5CoCrFeNi high-entropy alloy: Corrosion behavior. *J. Alloys Compd.* **2020**, *817*, 153163. [CrossRef]
65. Sokkalingam, R.; Muthupandi, V.; Sivaprasad, K.; Prashanth, K.G. Dissimilar welding of $Al_{0.1}$CoCrFeNi high-entropy alloy and AISI304 stainless steel. *J. Mater. Res.* **2019**, 1–12. [CrossRef]
66. Sokkalingam, R.; Mishra, S.; Cheethirala, S.R.; Muthupandi, V.; Sivaprasad, K. Enhanced Relative Slip Distance in Gas-Tungsten-Arc-Welded Al0.5CoCrFeNi High-Entropy Alloy. *Metall. Mater. Trans. A* **2017**, *48*, 3630–3634. [CrossRef]

67. Martin, A.C.; Fink, C. Initial weldability study on $Al_{0.5}CrCoCu_{0.1}FeNi$ high-entropy alloy. *Weld. World* **2019**, *63*, 739–750. [CrossRef]
68. Martin, A.C.; Oliveira, J.P.; Fink, C. Elemental Effects on Weld Cracking Susceptibility in $Al_xCoCrCu_yFeNi$ High-Entropy Alloy. *Metall. Mater. Trans. A* **2019**, *51*, 778–787. [CrossRef]
69. Panina, E.; Yurchenko, N.; Zherebtsov, S.; Stepanov, N.; Salishchev, G.; Ventzke, V.; Dinse, R.; Kashaev, N. Laser Beam Welding of a Low Density Refractory High Entropy Alloy. *Metals* **2019**, *9*, 1351. [CrossRef]
70. Wang, P.; Huang, P.; Ng, F.L.; Sin, W.J.; Lu, S.; Nai, M.L.S.; Dong, Z.L.; Wei, J. Additively manufactured CoCrFeNiMn high-entropy alloy via pre-alloyed powder. *Mater. Des.* **2019**, *168*, 107576. [CrossRef]
71. Wang, B.; Yao, X.; Wang, C.; Zhang, X.; Huang, X. Mechanical properties and microstructure of a NiCrFeCoMn high-entropy alloy deformed at high strain rates. *Entropy* **2018**, *20*, 892. [CrossRef]
72. Ma, D.; Grabowski, B.; Körmann, F.; Neugebauer, J.; Raabe, D. Ab initio thermodynamics of the CoCrFeMnNi high entropy alloy: Importance of entropy contributions beyond the configurational one. *Acta Mater.* **2015**, *100*, 90–97. [CrossRef]
73. Subrahmanyam, J.; Vijayakumar, M. Self-propagating high-temperature synthesis. *J. Mater. Sci* **1992**, *27*, 6249–6273. [CrossRef]
74. Wang, Z.; Oliveira, J.P.; Zeng, Z.; Bu, X.; Peng, B.; Shao, X. Laser beam oscillating welding of 5A06 aluminum alloys: Microstructure, porosity and mechanical properties. *Opt. Laser Technol.* **2019**, *111*, 58–65. [CrossRef]
75. Gu, J.; Ni, S.; Liu, Y.; Song, M. Regulating the strength and ductility of a cold rolled FeCrCoMnNi high-entropy alloy via annealing treatment. *Mater. Sci. Eng. A* **2019**, *755*, 289–294. [CrossRef]
76. Khodabakhshi, F.; Gerlich, A.P. On the stability, microstructure, and mechanical property of powder metallurgy Al–SiC nanocomposites during similar and dissimilar laser welding. *Mater. Sci. Eng. A* **2019**, *759*, 688–702. [CrossRef]
77. Otto, F.; Dlouhý, A.; Somsen, C.; Bei, H.; Eggeler, G.; George, E.P. The influences of temperature and microstructure on the tensile properties of a CoCrFeMnNi high-entropy alloy. *Acta Mater.* **2013**, *61*, 5743–5755. [CrossRef]
78. Montazeri, M.; Ghaini, F.M.; Farnia, A. An investigation into the microstructure and weldability of a tantalum-containing cast cobalt-based superalloy. *Int. J. Mater. Res.* **2011**, *102*, 1446–1451. [CrossRef]
79. Henderson, M.B.; Arrell, D.; Larsson, R.; Heobel, M.; Marchant, G. Nickel based superalloy welding practices for industrial gas turbine applications. *Sci. Technol. Weld. Joining* **2004**, *9*, 13–21. [CrossRef]
80. Elangovan, K.; Balasubramanian, V. Influences of post-weld heat treatment on tensile properties of friction stir-welded AA6061 aluminum alloy joints. *Mater. Charact.* **2008**, *59*, 1168–1177. [CrossRef]
81. Köse, C.; Kaçar, R. The effect of preheat & post weld heat treatment on the laser weldability of AISI 420 martensitic stainless steel. *Mater. Des.* **2014**, *64*, 221–226.
82. Oliveira, J.P.; Panton, B.; Zeng, Z.; Andrei, C.M.; Zhou, Y.; Miranda, R.M.; Fernandes, F.M.B. Laser joining of NiTi to Ti6Al4V using a Niobium interlayer. *Acta Mater.* **2016**, *105*, 9–15. [CrossRef]
83. Miranda, R.M.; Assunção, E.; Silva, R.J.C.; Oliveira, J.P.; Quintino, L. Fiber laser welding of NiTi to Ti-6Al-4V. *In. J. Adv. Manuf. Technol.* **2015**, *81*, 1533–1538. [CrossRef]
84. Young, G.A.; Capobianco, T.E.; Penik, M.A.; Morris, B.W.; McGee, J.J. The mechanism of ductility dip cracking in nickel-chromium alloys. *Weld. J.* **2008**, *87*, 31S–43S.
85. Ramirez, A.J.; Sowards, J.W.; Lippold, J.C. Improving the ductility-dip cracking resistance of Ni-base alloys. *J. Mater. Process. Technol.* **2006**, *179*, 212–218. [CrossRef]
86. Xu, N.; Song, Q.; Bao, Y. Microstructure evolution and mechanical properties of friction stir welded FeCrNiCoMn high-entropy alloy. *Mater. Sci. Technol.* **2019**, *35*, 577–584. [CrossRef]
87. Zhu, Z.G.; Sun, Y.F.; Goh, M.H.; Ng, F.L.; Nguyen, Q.B.; Fujii, H.; Nai, S.M.L.; Wei, J.; Shek, C.H. Friction stir welding of a $CoCrFeNiAl_{0.3}$ high entropy alloy. *Mater. Lett.* **2017**, *205*, 142–144. [CrossRef]
88. Zhu, Z.G.; Sun, Y.F.; Ng, F.L.; Goh, M.H.; Liaw, P.K.; Fujii, H.; Nguyen, Q.B.; Xu, Y.; Shek, C.H.; Nai, S.M.L.; et al. Friction-stir welding of a ductile high entropy alloy: microstructural evolution and weld strength. *Mater. Sci. Eng. A* **2018**, *711*, 524–532. [CrossRef]
89. Park, S.; Park, C.; Na, Y.; Kim, H.S.; Kang, N. Effects of (W, Cr) carbide on grain refinement and mechanical properties for CoCrFeMnNi high entropy alloys. *J. Alloys Compd.* **2019**, *770*, 222–228. [CrossRef]
90. Shaysultanov, D.; Stepanov, N.; Malopheyev, S.; Vysotskiy, I.; Sanin, V.; Mironov, S.; Kaibyshev, R.; Salishchev, G.; Zherebtsov, S. Friction stir welding of a carbon-doped CoCrFeNiMn high-entropy alloy. *Mater. Charact.* **2018**, *145*, 353–361. [CrossRef]

91. Li, P.; Sun, H.; Wang, S.; Hao, X.; Dong, H. Rotary friction welding of $AlCoCrFeNi_{2.1}$ eutectic high entropy alloy. *J. Alloys Compd.* **2020**, *814*. [CrossRef]
92. Lei, Y.; Hu, S.P.; Yang, T.L.; Song, X.G.; Luo, Y.; Wang, G.D. Vacuum diffusion bonding of high-entropy $Al_{0.85}CoCrFeNi$ alloy to TiAl intermetallic. *J. Mater. Process. Technol.* **2020**, *278*, 116455. [CrossRef]
93. Oliveira, J.P.; Duarte, J.F.; Inácio, P.; Schell, N.; Miranda, R.M.; Santos, T.G. Production of Al/NiTi composites by friction stir welding assisted by electrical current. *Mater. Des.* **2017**, *113*, 311–318. [CrossRef]
94. Khan, N.Z.; Siddiquee, A.N.; Khan, Z.A.; Shihab, S.K. Investigations on tunneling and kissing bond defects in FSW joints for dissimilar aluminum alloys. *J. Alloys Compd.* **2015**, *648*, 360–367. [CrossRef]
95. Costa, A.M.S.; Oliveira, J.P.; Pereira, V.F.; Nunes, C.A.; Ramirez, A.J.; Tschiptschin, A.P. Ni-based Mar-M247 superalloy as a friction stir processing tool. *J. Mater. Process. Technol.* **2018**, *262*, 605–614. [CrossRef]
96. Yan, H.; Fan, J.; Han, Y.; Yao, Q.; Liu, T.; Lv, Y.; Zhang, C. Vacuum diffusion bonding W to W-Cu composite: Interfacial microstructure and mechanical properties. *Vacuum* **2019**, *165*, 19–25. [CrossRef]
97. Zhang, P.; Li, Y.; Chen, Z.; Zhang, J.; Shen, B. Oxidation response of a vacuum arc melted NbZrTiCrAl refractory high entropy alloy at 800–1200 °C. *Vacuum* **2019**, *162*, 20–27. [CrossRef]
98. Yao, Q.; Cheng, H.; Fan, J.; Yan, H.; Zhang, C. High strength Mo/Ti6Al4V diffusion bonding joints: Interfacial microstructure and mechanical properties. *Int. J. Refract. Met. Hard Mater* **2019**, *82*, 159–166. [CrossRef]